

Nanoscale

Accepted Manuscript



This is an *Accepted Manuscript*, which has been through the Royal Society of Chemistry peer review process and has been accepted for publication.

Accepted Manuscripts are published online shortly after acceptance, before technical editing, formatting and proof reading. Using this free service, authors can make their results available to the community, in citable form, before we publish the edited article. We will replace this *Accepted Manuscript* with the edited and formatted *Advance Article* as soon as it is available.

You can find more information about *Accepted Manuscripts* in the [Information for Authors](#).

Please note that technical editing may introduce minor changes to the text and/or graphics, which may alter content. The journal's standard [Terms & Conditions](#) and the [Ethical guidelines](#) still apply. In no event shall the Royal Society of Chemistry be held responsible for any errors or omissions in this *Accepted Manuscript* or any consequences arising from the use of any information it contains.

Novel Sodium/Lithium-ion Anode Material Based on Ultrathin $\text{Na}_2\text{Ti}_2\text{O}_4(\text{OH})_2$ Nanosheet

Yuping Zhang,^a Lin Guo,^{a *} Shihe Yang^{a,b*}

^{a *} School of Chemistry and Environment, Beihang University, Beijing, 100191, P. R. China. E-mail: guolin@buaa.edu.cn

^b Department of Chemistry, The Hong Kong University of Science and Technology, Clear Water Bay, Kowloon Hong Kong (P.R. China). E-mail : chsyang@ust.hk

Abstract

Ultrathin $\text{Na}_2\text{Ti}_2\text{O}_4(\text{OH})_2$ nanosheets with ~8 nm was prepared by a facile method for first time. The as resulted material was also used as conducting agent and binder-free anode both for sodium ion batteries and lithium ion batteries for first time. The $\text{Na}_2\text{Ti}_2\text{O}_4(\text{OH})_2$ nanosheets exhibit excellent Na/Li-ion storage performance. The long-term cycling performance of ultrathin $\text{Na}_2\text{Ti}_2\text{O}_4(\text{OH})_2$ nanosheets of 120 mAh g⁻¹ at ~10C was retained after 500 cycles for sodium ion batteries, and 150 mAh g⁻¹ at ~1C was kept after 500 cycles for lithium ion batteries. By comparison, the Na-ion storage performance is much better than Li-ion storage performance over $\text{Na}_2\text{Ti}_2\text{O}_4(\text{OH})_2$ nanosheets anode for the existence of Na in host of $\text{Na}_2\text{Ti}_2\text{O}_4(\text{OH})_2$.

KEYWORDS: $\text{Na}_2\text{Ti}_2\text{O}_4(\text{OH})_2$, Nanosheet, Anode, Sodium ion batteries, Lithium ion batteries.

Introduction

Nowadays world is full of extensive energy consumption and most usage closed

with our daily lives. To alleviate this extensively energy demand, energy storage plays a more and more important role in the world.¹⁻³ The art of rechargeable batteries⁴⁻⁸ is one of techniques for electrical energy storage. Among all these rechargeable batteries recently, lithium ion batteries (LIBs) with the advantage of high energy density have received worldwide attention, especially for the future application in portable electronics, electric vehicles and grid storage, and a lot of great efforts have been made.⁹⁻¹³ Moreover, increased attentions are also focused on sodium ion batteries (SIBs) due to their cost-effectiveness preferable to the Li-ion counterparts.¹⁴⁻¹⁹

Regardless of the application, to discover and optimize the high performance electrode material is most important for developing both the Li-ion and Na-ion rechargeable battery technologies. Generally speaking, the metallic or semi-metallic redox cations located in s, p, d, and f blocks are suitable used as electrode material. However, the literature about same material used as electrode both for LIBs and SIBs is not enough reported. Recently, a kind of host materials has been reported as cathode both for SIBs and LIBs.²⁰ In addition, a few variety of metal oxides including $\alpha\text{-Fe}_2\text{O}_3$ ²¹⁻²³, Sb_2O_x ^{24,25}, SnO_2 ^{26,27}, MoO_3 ^{28,29}, V_2O_5 ^{30,31} and TiO_2 ^{32,33} can be used as electrode both for LIBs and SIBs. Because of the difference between in the ionic size of Li (0.076 nm) and Na (0.102nm), exploring the multipurpose layered material used not only for LIBs, but also for SIBs is still great challenge for the researchers. Moreover, the new electrode materials with unique structure benefiting the Li/Na-ion diffusion are also deserved to be designed and explored.

Recently, two-dimensional (2D) nanosheets have aroused tremendous interests in

Li/Na-ion batteries, due to the miniscule atomic scale thicknesses path for fast Na and Li ion diffusion, and large exposed surface offering enough channels for ions inserting into the host of electrode. Moreover, such ultrathin nanosheets build large open space to hold the droplet of electrolyte which may also reduce the electrode polarization when fast lithium or sodium storage.³⁴⁻³⁸ 2D nanosheets constructed Ti-containing species^{35,39,40} exhibited much excellent Li-ion storage performance were also reported. By comparison, the literature associated with the 2D nanosheets material as electrode for SIBs is far less reported than that for LIBs. Therefore, it is still highly desirable to develop and explore more and more 2D nanosheets electrode both for LIBs and SIBs, due to their unique structure advantage for Li/Na-ion diffusion and insertion.

Herein, ultrathin $\text{Na}_2\text{Ti}_2\text{O}_4(\text{OH})_2$ (NTOH) nanosheets with ~ 8 nm thickness is synthesized by alkali-treated Ti foil in hydrothermal atmosphere. The resultant material without any additional conducting agent and binder exhibits excellent electrochemical performance as anode both for SIBs and LIBs for first time. The reversible capacity of 400 mAh g^{-1} , and 600 mAh g^{-1} are obtained at 0.23C ($1\text{C} = 216 \text{ mA g}^{-1}$) can be retained over LIBs and SIBs, respectively. Long-term cyclic stability is also exhibited by NTOH nanosheets over LIBs and SIBs, 120 mAh g^{-1} at $\sim 10\text{C}$ was retained after 500 cycles for SIBs, and 150 mAh g^{-1} at $\sim 1\text{C}$ was kept after 500 cycles for LIBs. The electrochemical performance of NTOH for SIBs is much better than that of LIBs due to more Na^+ can inserts into the frame of than Li^+ .

Experimental section

Electrode preparation: The ultrathin NTOH electrodes were synthesized by alkali

treatment of Ti flake in a diluted sodium hydroxide solution similar as our previous work.¹⁴ In a typical preparation, one piece of titanium foil (3 cm × 2 cm × 0.3 mm) was ultrasonically cleaned in acetone, ethanol and water for half an hour, respectively. Then, placing Ti plate against the wall of a 40 mL volume of Teflon-lined stainless steel autoclave, filled with 30 mL 1 M NaOH solution, and then sealed the autoclave and kept the autoclave at 200 °C for 20 hours. After the hydrothermal growth and cooling down to room temperature, the Ti plate was taken out, and rinsed with distilled water for several times, further dried at 60 °C for several hours, and NTOH electrodes were obtained.

Materials Characterization: The crystal structures of the as-obtained T_n were characterized by X-ray powder diffraction (XRD) using a Shimadzu X-Lab6000 X-ray diffractometer with Cu $K\alpha$ radiation ($\lambda = 1.5416 \text{ \AA}$). The morphology of T_n structure was taken by using a JEOL JSM-7001F field emission scanning electron microscope (SEM). The element composition of as-prepared samples was analyzed by a JEOL JSM-7500F cold-field emission scanning electron microscope (CFESEM) and its affiliated energy dispersive X-ray diffraction spectroscopy (EDS). Transmission electron microscopy (TEM), high-resolution transmission electron microscopy (HRTEM) images, and the selected area electron diffraction (SAED) pattern were obtained by using a JEOL JEM-2100F microscope. The IR spectra was determined by using a iN10MX micro infrared spectrometer in the range of 4000-500 cm^{-1} . Raman spectra was studied on a LabRAM HR800 Renishaw confocal Raman micro-spectroscopy with 514 nm laser radiation in the range of 100–1000 cm^{-1} .

Atomic Force Microscope (AFM) image was obtained from a tapping mode with a commercial multimode Nanoscope IIIa (Veeco Co. Ltd). ICP analysis was obtained from the Agilent ICP-MS7500Ce instrument. XPS spectra were determined by ThermoFisher ESCALAB250Xi X-ray photoelectron spectroscopy.

Electrochemical Measurement: Electrochemical experiments tests were performed by using the coin cells (CR 2032). One side of NTOH material was scraped away by using doctor blade so as to expose the Ti substrate as current collector. Then, the electrode was successfully prepared. The sodium metal and lithium metal acted as the counter and reference electrodes for SIBs, LIBs. Borosilicate glass fibers (GF/D) from Whatman were used as separators, and the cells were assembled in an Ar-filled glove box. The Charge-discharge measurements were carried out on CT2001A Land battery testing systems (Jinnuo Electronics Co. Ltd., China) at different current density in a potential range of 0.01-2.5 V vs. Na/Na⁺. Cyclic voltammetry (CV) curves were collected from CHI660D electrochemical workstation at 0.1 mV/s within the range of 0.01-2.5 V. Electrochemical impedance spectroscopy (EIS) was also carried out on the CHI660D electrochemical workstation at an open circuit voltage, with an AC voltage of 5 mV, and in the frequency range of 100 kHz to 0.01 Hz.

Results and Discussion

X-ray diffraction (XRD) technique was used to determine the crystallographic structure and the XRD pattern belongs to Na₂Ti₂O₄(OH)₂ as shown in **Figure S1**(Supporting Information). The EDS spectroscopy shown in **Figure S2** is also confirmed that the elements of Ti, Na, O in the ultrathin nanosheets, and the atomic

ration of Na/Ti is 1.02, which is completely approaching to that in NTOH. In addition, ICP measurement of Na/Ti ration is equal to 0.98, which is further confirmed the existence of NTOH. The IR spectroscopy shown in **Figure S3** clearly confirms the -OH existed in $\text{Na}_2\text{Ti}_2\text{O}_4(\text{OH})_2$. The Raman spectra were also shown in **Figure S4** and **S5**. Furthermore, XPS spectra in Figure S6 The was shown the information of chemical state for Na, Ti, and O in $\text{Na}_2\text{Ti}_2\text{O}_4(\text{OH})_2$ materials.

The morphology of as prepared NTOH sample was studied by scanning electron microscopy (SEM). As shown in **Figure 1a**, the thickness of the ultrathin NTOH layer grown on Ti-foil substrate is approaching to $\sim 4 \mu\text{m}$. The layer was evenly assembled by a large quantity of ultrathin NTOH nanosheets as shown in the inset of **Figure 1a**, and clearly exhibits in **Figure 1b**. In addition, when we divert our attentions to the thickness of the ultrathin NTOH nanosheets themselves, these nanosheets were $\sim 8 \text{ nm}$ in thickness on average as shown in **Figure 1c** and **Figure 1d**, Furthermore, the width of these nanosheets was over at least $1 \mu\text{m}$, and no coalescence between the neighbors on the top of the layer as displayed in **Figure 1d**. In addition, the thickness and width of NTOH nanosheets are further confirmed by using three-dimensional AFM images as shown in **Figure 1e** and **Figure 1f**. From the SEM images of the cross-section and the surface of the NTOH on the Ti-foil substrate, a common character was appeared in our eyes, these loose ultrathin nanosheets were vertically distributed on the surface of Ti substrate, providing large enough open space between neighboring nanosheets.

Transmission electron microscopy (TEM) was performed using to further investigate the more details of morphology and structure for those ultrathin NTOH

nanosheets. As shown in **Figure 2a** and **Figure 2b** of TEM images, the as prepared ultrathin NTOH nanosheets exhibits in two-dimensional (2D) with smooth surface as soft silk-like, which agrees with that of above SEM images. Due to too small thickness, some of the nanosheets gradually scrolled into one-dimensional (1D) state as denoted in **Figure 2a** and **2b**. In addition, HRTEM in **Figure 2d** together with SAED (inset of **Figure 2c**) show that the ultrathin NTOH nanosheets exhibits good crystallization. The nanosheets display different lattice fringe spacing of 0.19 nm and 0.42 nm, which respectively index to (110) and (701) planes of NTOH. However, the ultrathin nanosheet of NTOH is very sensitive to the electron beaming during the TEM image taken. The amorphous state was quick formed where the electron beaming focused on, which is also reflected in the HRTEM image of **Figure 2d**. In addition, EDX elemental mapping in **Figure 2e** are clearly shown that the element of Na, Ti, and O are evenly distributed in the NTOH nanosheets.

The ultrathin NTOH nanosheets were directly used as binder-free and conducting agent-free anode for electrochemical test of Li-storage and Na-storage. The cyclic voltammetry (CV) was firstly carried out to examine the lithium/sodium ion insertion properties of the NTOH electrode. **Figure 3A** shows the CV plot of ultrathin NTOH nanosheet as anode for LIBs at a scan rate of 0.1 mV s^{-1} over the potential window of 0.01-3 V (vs Li/Li⁺). Two couples of redox peaks are observed from the CV curve, the good repeatability of cathodic/anodic peaks confirms the great reaction reversibility of as prepared ultrathin NTOH nanosheets anode. One couple redox peaks is around 0.2 V, this redox peaks exhibits the higher intensity reductive peak than oxidation peak,

indicating that Li^+ insertion process is more easily conducted than Li^+ extraction process, this may be ascribed to that the Solid Electrolyte Interface (SEI) film formed, or some side reactions are taken. Another obvious anodic/cathodic peak located around 1.5-1.8 V can be ascribed to the redox reaction of $\text{Ti}^{4+}/\text{Ti}^{3+}$ during the lithium insertion/extraction process.^{41,42} It is also note that the great overlap and same intensity of oxidation peak during the first four times scanning cycle. However, the intensity of reduction peak is gradually strengthened as cycle increasing up, indicating that more and more Li^+ are inserted into the frame of NTOH. Different from that of Li-ion batteries, **Figure 3B** shows CV file of ultrathin NTOH nanosheet as anode for SIBs. As shown in **Figure 3B**, there is a couple redox peaks observed between 0.2-0.5 V (vs Na/Na^+), which is ascribed to the redox reaction of $\text{Ti}^{4+}/\text{Ti}^{3+}$ during the process of charging/discharging.⁴³⁻⁴⁵ The reductive peak at 0.22 V is assigned to Na^+ inserted into the lattice of NTOH, while the oxidative peak at ~ 0.5 V indicates that Na^+ extracted from the lattice of fully discharged NTOH. In addition, the reductive peak gradually shrink is due to the formation of SEI film in the initial cycling. **Figure 3C** shows the Nyquist plots obtained from experiment of ultrathin NTOH nanosheets electrodes both from the fresh cell of LIBs and SIBs. For the experimental or simulated EIS plots of lithium ion batteries, there is only one depressed semicircle in the high-to-middle frequency region, plus an inclined line in low frequency region. However, the EIS curve for SIBs is a bit difference from that of LIBs, there are two semicircles appearing from the high frequency and middle frequency regions, respectively. In addition, the impedance plots were fitted using the equivalent circuit

model as shown in inset of **Figure 3C**, and impedance parameters calculated from equivalent circuits from fresh cell of SIBs and LIBs is shown in **Table S1**. The intercept at the Z' axis in high frequency region corresponded to ohmic resistance (R_e), which related with the resistance of electrolyte. As observed the diameter of semicircle from the high frequency region in EIS of LIBs and SIBs, we find that the R_e for LIBs can be omit compare with that for SIBs, indicating that the diffusion of Na^+ in ethylene carbonate/dimethyl carbonate electrolyte solution is more difficult than Li^+ . The semicircle in middle frequency region represented the charge transfer resistance (R_{st}). As observed the diameter of this semicircle, we can also find that the R_{st} for SIBs is much bigger than that of LIBs. CPE represents the constant phase-angle element, involving double-layer capacitance, and the inclined line in low frequency region indicated the Warburg impedance (Z_w), which are mostly associated with Na^+ or Li^+ diffusion in the ultrathin NTOH nanosheet anode.

Aforementioned CV had been primarily analyzed the electrochemical performance of the ultrathin NTOH nanosheets, and we will continue investigate its ion-storage property. As observed from the **Figure 4a** and **Figure 4b**, in the voltage window of 0.005-2.5 V, the binder-free and conducting agent-free ultrathin NTOH nanosheets anode deliver the initial discharge capacity of 1200 mAh g^{-1} and 800 mAh g^{-1} for SIBs and LIBs respectively at the current density of 50 mA g^{-1} . While their counterpoint charge capacities are respectively 720 and 580 mAh g^{-1} , much lower than that of discharge capacity. As the above CV plots reflected, indicating that the formation of SEI film contributed the higher initial discharge capacity in the process.

However, when the cycling turns to second, the charge and discharge capacity are much closer each other. The specific capacity is kept at 500 mAh g^{-1} for LIBs, and 750 mAh g^{-1} is obtained from the SIBs. Both the capacities show bit decay when the discharge/charge process running to the third cycle, but the specific capacity could be still kept above 600 mAh g^{-1} and 400 mAh g^{-1} for SIBs and LIBs, respectively. Moreover, the rate capability of ultrathin NTOH nanosheet anode over SIBs and LIBs show in **Figure 4c** and **Figure 4d**. As shown in **Figure 4c**, the anode delivers the stable discharge capacity of 570, 360, 330, 300, 270, 250, 220 and 200 mAh g^{-1} at the current density of 50, 100, 200, 500, 800, 1000, 2000, and 3000 mA g^{-1} over the Na-ion batteries. When the cycling recovers back from the high current density of 3000 mA g^{-1} to 50 mA g^{-1} , the discharge capacity still keeps at 500 mAh g^{-1} . By contrast, the rate performance of the NTOH anode for LIBs were much lower than that of SIBs, and the discharge capacity at different current density of 25, 50, 100, 200, 500, 800, 1000, 2000, and 3000 mA g^{-1} were almost below 200 mAh g^{-1} , except at the C-rate of $\sim 0.1\text{C}$ (25 mA g^{-1}). As a result, the rate capability for NTOH anode both for SIBs and LIBs exhibit much better performance and stability at high C-rate than at low current density, especially for the cell of the SIBs. In addition, the long-term cycling performance are shown in **Figure 4e** and **Figure 4f**, the reversible specific capacity of 120 mAh g^{-1} can be retained over the SIBs at the current density of 2000 mA g^{-1} over 500 cycles, companying with the coulombic efficiency of 65% at the initial cycling increased to 100%. Moreover, considering the much low capacity of the anode over the LIBs, the test of long life cycling performance for LIBs was carried

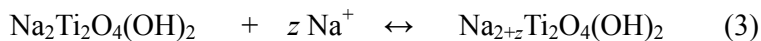
out at the current density of 200 mA g^{-1} . As shown in **Figure 4f**, the reversible specific capacity of 150 mAh g^{-1} can be retained over 500 cycles over Li-ion cell, and the accompanying the almost 100% coulombic efficiency. As a result, the long-term cycling capability is also excellent for the ultrathin NTOH anode both over LIBs and SIBs, as well as that of great reversible capacity and good rate capability. What is more, such excellent Li/Na-storage property of the ultrathin NTOH nanosheets may also result from the unique structure, the art of ultrathin 2D NTOH supplies the shortest path for Na or Li ions diffusion, and the no connected neighboring nanosheets construct large open space used for electrolyte reservoiring. All this complex factors contribute the great electrochemical ion-storage performance of NTOH. In comparison with other reports on various materials both for SIBs and LIBs, the as-prepared NTOH nanosheets delivers high capacity, great cycling performance and rate capability (Table S2).^{26,27,30-33}

According to the CV data and the ion-storage performance of the ultrathin NTOH nanosheets in the Na-cell and Li-cell, it is inferred that the as prepared material is a promising electrode both for sodium-ion batteries and lithium-ion batteries. Herein, we are also interested in the ion-storage mechanism over the ultrathin NTOH nanosheets. As well known, the property of a chemical material was always closely associated with its structure. The crystal structure of $\text{Na}_2\text{Ti}_2\text{O}_4(\text{OH})_2$ is shown in **Figure 5**, $\text{Na}_2\text{Ti}_2\text{O}_4(\text{OH})_2$ belongs to the body-centered orthorhombic crystal structure with unit cell of $a = 1.926 \text{ nm}$, $b = 0.378 \text{ nm}$ and $c = 0.300 \text{ nm}$, the unit of TiO_6 octahedra is separated by the layer of Na^+ . Benefiting from the layer structure of

$\text{Na}_2\text{Ti}_2\text{O}_4(\text{OH})_2$, the Li^+ or Na^+ can be easily inserted/extracted into/out of the layer, and the feasibility of Li-ion or Na-ion storage is come ture. As Na^+ are replaced by the Li^+ when the NTOH is used as an anode for the lithium ion battery during the discharge process, and insertion and extraction of the Li^+ ion are respectively shown as below equation :



Equation 1 is an irreversible reaction (The Raman spectra somehow prove this irreversiable reaction as shown in **Figure S4**) describing the Li^+ exchange with Na^+ during the initial discharge process, which belongs to conversion reaction, and this initial ion exchange donates the basic Li-ion storage capacity of the cell. Then the Li^+ extracted from the full-discharged NTOH electrode during the charge process. After that, only Li^+ insert or extract into/from the frame of NTOH during the redox change of $\text{Ti}^{4+}/\text{Ti}^{3+}$ as shown in **equation 2**. However, when $\text{Na}_2\text{Ti}_2\text{O}_4(\text{OH})_2$ was used as anode for sodium ion battery, the discharge and charge process are possibly described as follow **equation 3**.



Aforementioned that after the fully discharged of NTOH as anode for lithium ion battery, there are still some of Na^+ left in the frame of the $\text{Na}_{2-x}\text{Li}_x\text{Ti}_2\text{O}_4(\text{OH})_2$. However, the situation is changed when the NTOH used as anode for sodium ion battery, the ions of Na^+ in electrolyte insert into the frame of NTOH. NTOH is changing into the phase of $\text{Na}_{2+z}\text{Ti}_2\text{O}_4(\text{OH})_2$. The sodium content in fully discharged

$\text{Na}_{2+z}\text{Ti}_2\text{O}_4(\text{OH})_2$ in SIBs is much higher than the lithium content in fully Li-inserted $\text{Na}_{2-x}\text{Li}_x\text{Ti}_2\text{O}_4(\text{OH})_2$ (as also confirmed from the Raman spectra in **Figure 5S**). Therefore, the ions transfer in Li-storage is far less than that of Na-storage. This may be used to explain why the practical capacity of Na-ion battery is higher than Li-ion battery.

In summary, we have developed a novel ultrathin $\text{Na}_2\text{Ti}_2\text{O}_4(\text{OH})_2$ nanosheets anode by a simple hydrothermal route. Benefiting from the unique sheet structure of ultrathin thickness, the Na^+/Li^+ diffusion distance is significantly shortened for Li/Na-storage. Moreover, thanks to the large open space of the anode structure, the electrolyte is easily accessible to the nanosheets with good conductivity. The ultrathin $\text{Na}_2\text{Ti}_2\text{O}_4(\text{OH})_2$ nanosheets exhibit great Na-storage and Li-storage performance. Remarkable for Na-storage are the excellent specific capacity, high rate capability and good long-term cycling stability, which bode well for sodium ion batteries.

Acknowledgements

We acknowledge the National Natural Science Foundation of China (11079902, 51272012).

Reference

- [1] G. Zheng, S. W. Lee, Z. Liang, H.-W. Lee, K. Yan, H. Yao, H. Wang, W. Li, S. Chu, Y. Cui, *Nature Nanotech*, **2014**,9,618-623.
- [2] A. D. Roberts, X. Li, H. Zhang, *Chem.Soc.Rev.*, **2014**,43,4341-4356.
- [3] B. L. Ellis, L. F. Nazar, *Curr. Opin. Solid State Mater. Sci.*, **2012**,16,168-177.
- [4] Z. Li, J. Huang, B. Y. Liaw, V. Metzler, J. Zhang, *J. Power Sources*,

2014,254,168-182.

[5] A. C. Luntz, B. D. McCloskey, *Chem. Rev.*, **2014**,114, 11721-11750

[6] A. Manthiram, Y. Fu, S. Chung, C. Zu, Y.-S. Su, *Chem. Rev.*, **2014**,
114,11751-11787.

[7] P. G. Bruce, S. A. Freunberger, L. J. Hardwick¹, J.-M. Tarascon, *Nature Mater.*,
2012, 11,19-29.

[8] N. Yabuuchi, K. Kubota, M. Dahbi, S. Komaba, *Chem. Rev.*, **2014**,114,
11636-11682.

[9] T. Ohzuku, A. Ueda, *J. Electrochem. Soc.*, **1994**, 141,2972-2977.

[10] A. Yamada, S. C. Chung , K. Hinokuma, *J. Electrochem. Soc.*, **2001**,
148,A224-A229.

[11] D. K. Kim, P. Muralidharan, H.-W. Lee, R. Ruffo, Yuan Yang, C. K. Chan, H.
Peng, R. A. Huggins, Y. Cui, *Nano Lett.*, **2008**,8,3948-3952.

[12] H. Wang, L.-F. Cui, Y. Yang, H. S. Casalongue, J. T. Robinson, Y. Liang, Y. Cui,
H. Dai, *J. Am. Chem. Soc.*, **2010**, 132,13978-13980.

[13] G. Zhou, D.-W. Wang, F. Li, L. Zhang, N. Li, Z.-S. Wu, L. Wen, G. Q. Lu, H.-M.
Cheng, *Chem. Mater.*, **2010**,22, 5306-5313.

[14] Y. Zhang, L. Guo, S. Yang, *Chem. Commun.*, **2014**, 50,14029-14032.

[15] N. Yabuuchi ,M. Kajiyama, J. Iwatate, H. Nishikawa, S. Hitomi, R. Okuyama, R.
Usui, Y. Yamada, S. Komaba , *Nature Mater.* **2012**,11,512-517.

[16] S. Li, Y. Dong, L. Xu, X. Xu, L. He, L. Mai, *Adv. Mater.*, **2014**,26 ,3545-3553.

- [17] L. Wang, Y. Lu, J. Liu, M. Xu, J. Cheng, D. Zhang, *Angew. Chem. Int. Ed.*, **2013**, 52, 1964-1967.
- [18] Y. Wang, D. Su, C. Wang, G. Wang, *Electro. Commun.*, **2013**, 29, 8-11.
- [19] J. Qian, X. Wu, Y. Cao, X. Ai, H. Yang, *Angew. Chem.*, **2013**, 125, 4731-4734.
- [20] H. Kim, I. Park, D.-H. Seo, S. Lee, S.-W. Kim, W. J. Kwon, Y.-U. Park, C. S. Kim, S. Jeon, K. Kang, *J. Am. Chem. Soc.*, **2012**, 134, 10369-10372.
- [21] S. Komaba, T. Mikumo, N. Yabuuchi, A. Ogata, H. Yoshida, Y. Yamada, *J. Electrochem. Soc.*, **2010**, 157, A60
- [22] M. V. Reddy, T. Yu, C.-H. Sow, Z. X. Shen, C. T. Lim, G. V. Subba Rao, B. V. R. Chowdari, *Adv. Funct. Mater.*, **2007**, 17, 2792-2799.
- [23] X. Zhu, Y. Zhu, S. Murali, M. D. Stoller, R. S. Ruoff, *ACS Nano*, **2011**, 5, 3333-3338.
- [24] Q. Sun, Q.Q. Ren, H. Li, Z.W. Fu, *Electrochem Commun.*, **2011**, 13, 1462-1464.
- [25] H. Bryngelsson, J. Eskhult, L. Nyholm, M. Herranen, O. Alm, K. Edström, *Chem. Mater.*, **2007**, 19, 1170-1180.
- [26] J. Liang, Z. Cai, Y. Tian, L. Li, J. Geng, L. Guo, *ACS Appl. Mater. Interfaces.*, **2013**, 5, 12148-12155.
- [27] D. Su, H.-J. Ahn, G. Wang, *Chem. Commun.*, **2013**, 49, 3131-3133.
- [28] Y. Liu, B. H. Zhang, S. Y. Xiao, L. L. Liu, Z. B. Wen, Y. P. Wu, *Electrochimica Acta*, **2014**, 116, 512-517.
- [29] L. Mai, B. Hu, W. Chen, Y. Qi, C. Lao, R. Yang, Y. Dai, Z. L. Wang, *Adv. Mater.*, **2007**, 19, 3712-3716.

- [30] H. B. Wu, A. Pan, H. H. Hng, X. W. Lou, *Adv. Funct. Mater.*, **2013** ,23,5669-5674.
- [31] D. Su, G. Wang, *ACS Nano.*, **2013**,7,11218-11226.
- [32] Q. L. Wu, J. Li, R. D. Deshpande, N. Subramanian, S. E. Rankin, F. Yang, Y.-T. Cheng, *J. Phys. Chem. C.*, **2012** ,116 ,18669-18677.
- [33] H. Xiong, M. D. Slater, M. Balasubramanian, C.S. Johnson, T. Rajh, *J. Phys. Chem. Lett.*, **2011**, 2, 2560-2565.
- [34] J. Liu, X.-W. Liu, *Adv. Mater.*, **2012**,24,4097-4111.
- [35] S. Chen, Y. Xin, Y. Zhou, Y. Ma, H. Zhou, L. Qi, *Energy Environ. Sci.*, **2014**,7 ,1924-1930.
- [36] E. Yoo, J. Kim, E. Hosono, H. Zhou, T. Kudo, I. Honma, *Nano Lett.*, **2008** ,8,2277-2282.
- [37] W. Liu, Q. Sun, Y. Yang, J.-Y. Xie, Z.-W. Fu, *Chem. Commun.*, **2013** ,49,1951-1953.
- [38] D. Rangappa, K. D. Murukanahally, T. Tomai, A. Unemoto, I. Honma, *Nano Lett.*, **2012** ,12 ,1146-1151.
- [39] S. Liu, H. Jia, L. Han, J. Wang, P. Gao, D. Xu, J. Yang, S. Che, *Adv. Mater.*, **2012** ,24,3201-3204.
- [40] J. Chen, L. Yang, S. Fang, Y. Tang, *Electrochimica Acta* , **2010** ,55, 6596-6600.
- [41] L. Shen, E. Uchaker, X. Zhang, G. Cao, *Adv. Mater.*, **2012**,24, 6502-6506.
- [42] C. Qiu, Z. Yuan, L. Liu, S. Cheng, J. Liu, *Chin. J. Chem.*, **2013** ,31,819-825.

[43] H. Pan, X. Lu, X. Yu, Y. Hu, H. Li, X.-Q. Yang, L. Chen, *Adv. Energy Mater.*,

2013,3,1186-1194.

[44] A. Rudola, K. Saravanan, C. W. Masona, Palani Balaya, *J. Mater. Chem., A*,

2013,1, 2653-2662.

[45] W. Wang, C. Yu, Y. Liu, J. Hou, H. Zhu, S. Jiao, *RSC Adv.*, **2013**, 3,1041-1044.

Figure 1.

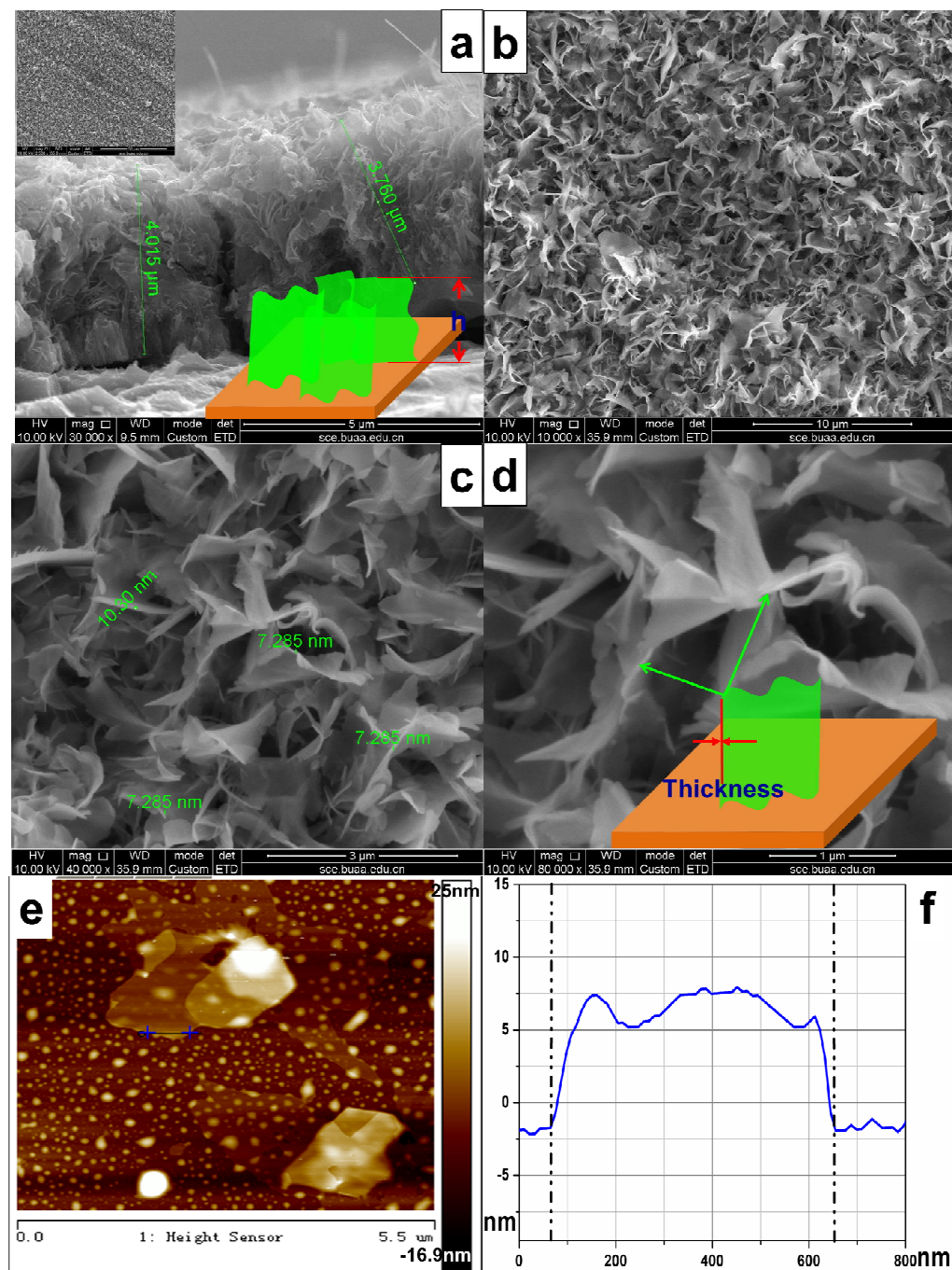


Figure 1. SEM images of as prepared NTOH sample: a) cross-section; b, c and d are SEM images at different resolution, e and f are AFM image of NTOH nanosheet .

Figure 2.

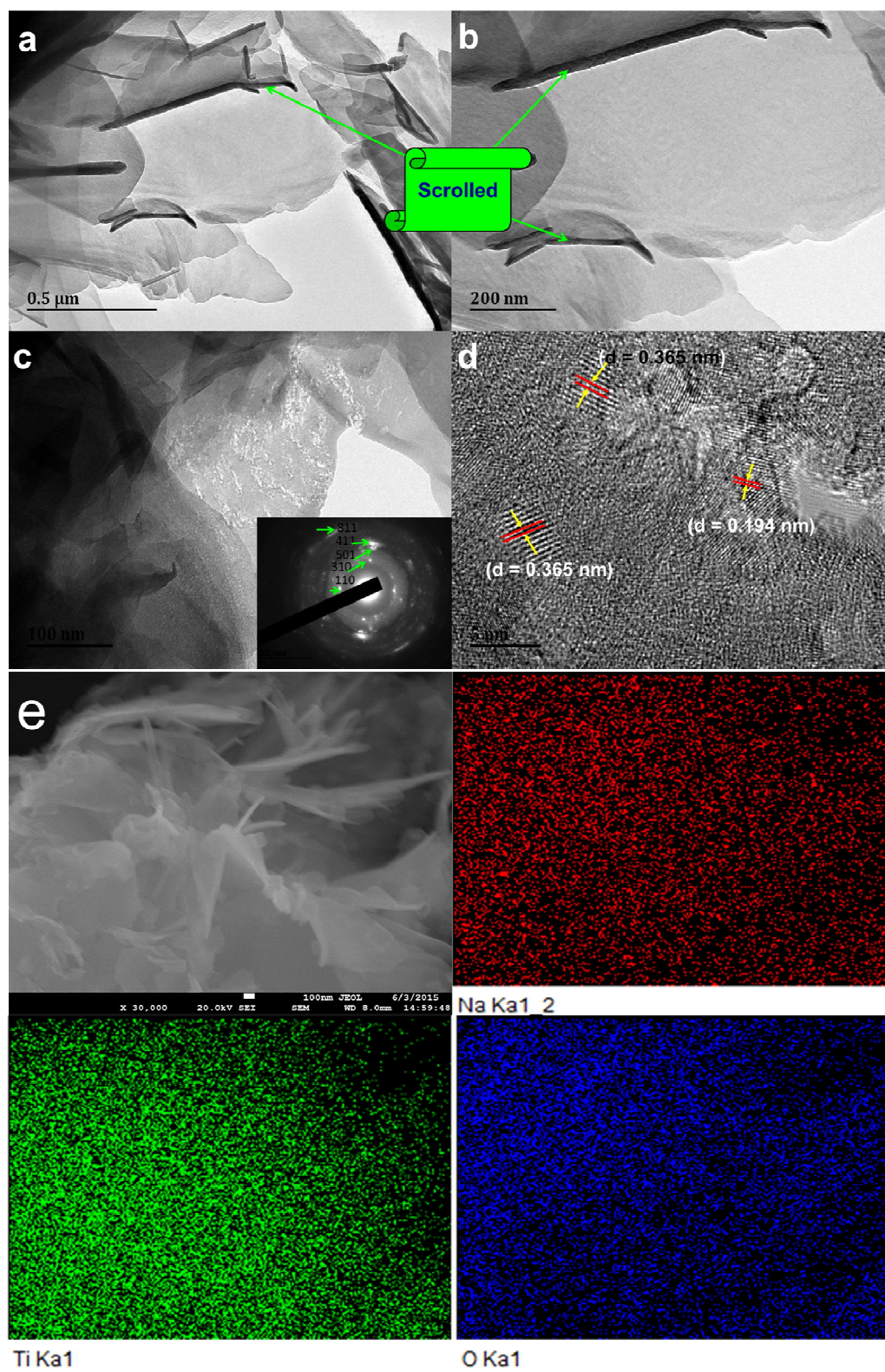


Figure 2. a, b and c) TEM image of as prepared NTOH nanosheets (inset of SAED in c); d) HRTEM image of NTOH nanosheets, e) EDX element mapping corresponding to Na, Ti and O in NTOH nanosheets.

Figure 3.

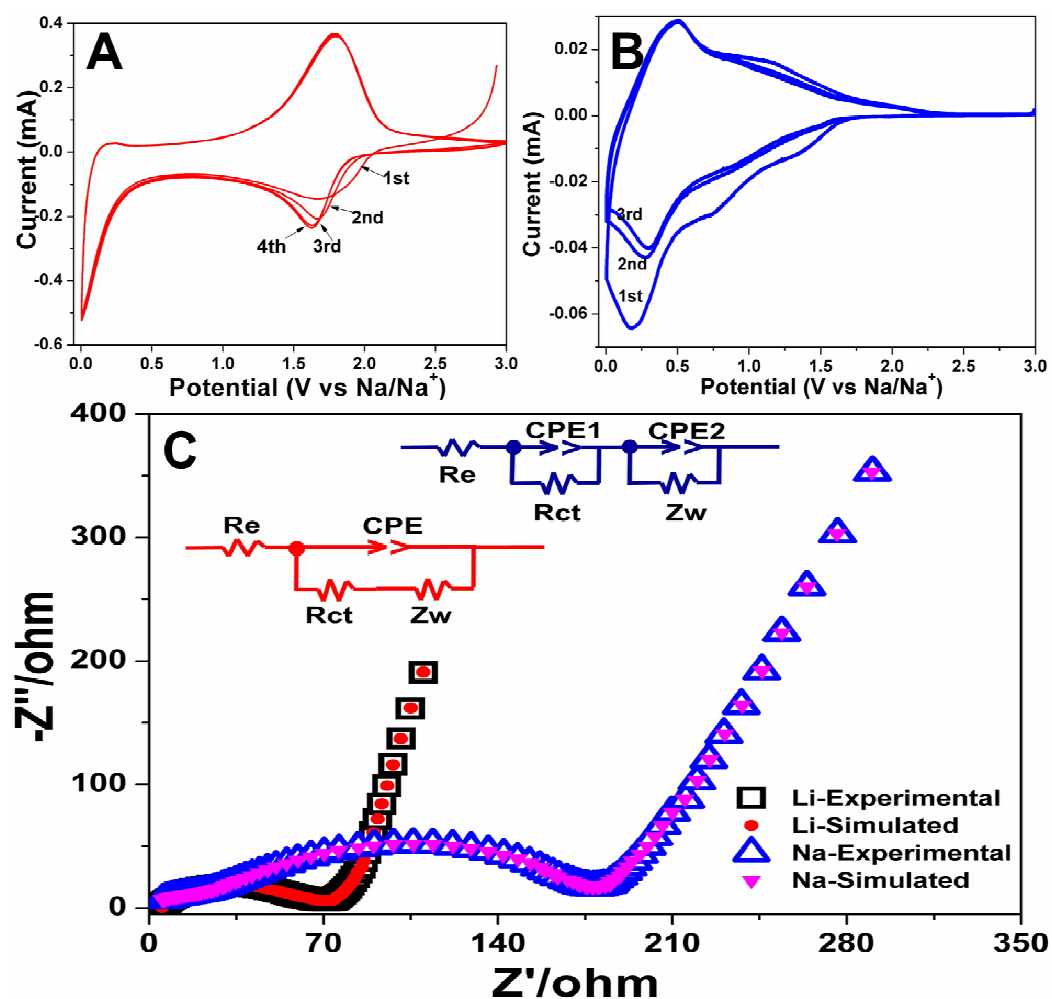


Figure 3. A) Cyclic voltammetry graph obtained from fresh LIBs coin cell; B) Cyclic voltammetry graph obtained from fresh SIBs coin cell; C) The experimental and simulated AC impedance spectra of NTOH anode on SIBs and LIBs, and the equivalent circuit.

Figure 4.

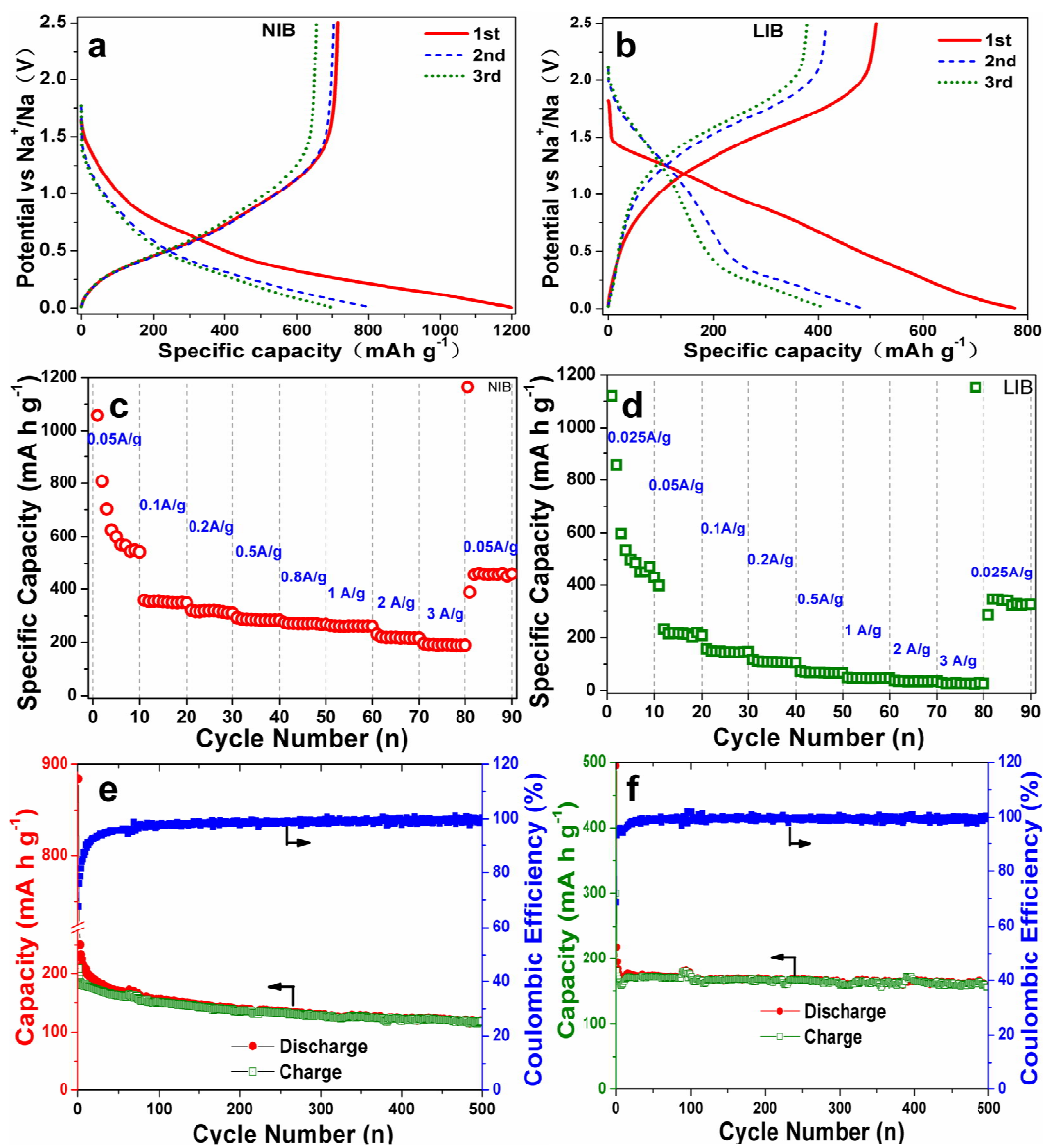


Figure 4. The first three discharge and charge curves of NTOH nanosheets for a) SIBs, b) LIBs; The rare capability of ultrathin NTOH nanosheets at different current density for c) SIBs, d) LIBs; Long-term cycling performance of NTOH nanosheets for e) SIBs, f) LIBs.

Figure 5

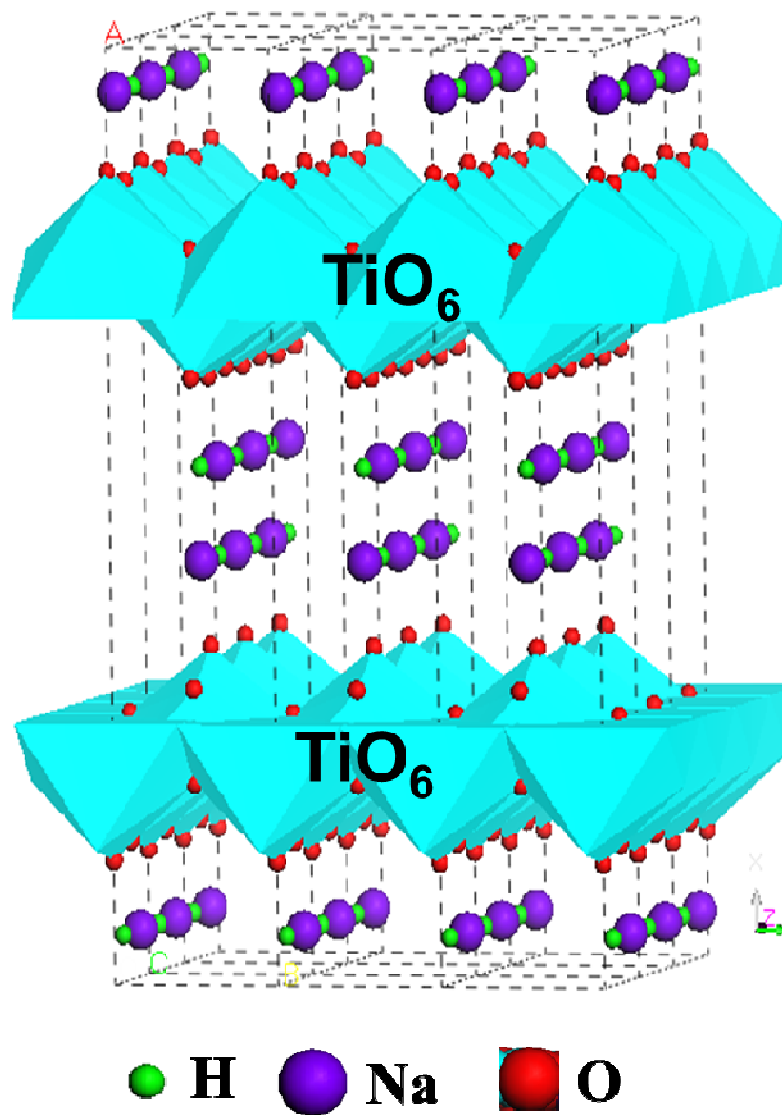


Figure 5. The crystal structure of $\text{Na}_2\text{Ti}_2\text{O}_4(\text{OH})_2$